ARTICLE

Check for updates

Rapid three-dimensional structuring of transparent SiO$_2$ glass using interparticle photo-cross-linkable suspensions

Ryoya Arita[1], Motoyuki Iijima [2✉], Yoko Fujishiro[1], Seitaro Morita[3], Taichi Furukawa[4], Junichi Tatami[2] & Shoji Maruo[4]

Photo-curable suspensions are important materials for shaping complex-structured ceramic and glass components. However, most systems undergo slow debinding and sintering so to avoid structural collapse by rapid gas generation from polymers. Here, we propose a new strategy to fabricate interparticle photo-cross-linkable suspensions for rapid three-dimensional structuring with short debinding and sintering times. SiO$_2$ particles modified with polyethyleneimine complexed with oleic acid (PEI-OA) are dispersed into a refractive-index-tuned solvent, where a photo-radical initiator and a lower-than-typical amount of multifunctional acrylates (MAs) were dissolved. The SiO$_2$ suspension is cured by the photo-radical polymerization of MA and the Michael additive reaction between polymerized MA and amino groups of PEI-OA on SiO$_2$ particles. These photo-curable suspensions can be employed in various shaping processes, from micro-scale stereolithography to centimeter-scale silicone molding. The SiO$_2$ green compacts with complex structures are also debinded and sintered into transparent glass components by rapid heating.

[1] Graduate School of Engineering Science, Yokohama National University, 79-5 Tokiwadai, Hodogayaku, Yokohama, Kanagawa 240-8501, Japan. [2] Faculty of Environment and Information Sciences, Yokohama National University, 79-7 Tokiwadai, Hodogayaku, Yokohama, Kanagawa 240-8501, Japan. [3] Graduate School of Environment and Information Sciences, Yokohama National University, 79-7 Tokiwadai, Hodogayaku, Yokohama, Kanagawa 240-8501, Japan. [4] Faculty of Engineering, Yokohama National University, 79-5 Tokiwadai, Hodogayaku, Yokohama, Kanagawa 240-8501, Japan. ✉email: iijima@ynu.ac.jp

Photo-curable suspensions have attracted extensive research attention as indispensable for designing complex-structured ceramics and glass components through additive manufacturing (e.g., digital light processing[1–8], laser-based stereolithography[9,10], mask projection stereolithography[11–14], suspension-enclosing projection stereolithography[15], and ultraviolet-assisted direct-write[16]), in-situ solidification[17,18], subtractive manufacturing[19], three-dimensional micro-template replication[20], fiber production[21], and stop-flow lithography[22]. Thus far, various photo-curable suspensions have been designed up to date. While the simplest process involves direct dispersion of inorganic fine particles in photo-curable monomers with photo-radical initiators[6–9,13–17,21,23–26], many researches have also focused on multi-component mixtures containing solvents to control suspension viscosities[1–5,10–12] and to form porosity in photo-cured green compacts which was favorable to debind polymers in a controlled manner[18]. Many further attempts have also made, such as by designing monomer mixtures to tune the number of reactive functional groups for controlling the photo-curing rates[23]; selecting monomers/solvents to achieve a transparent suspension and avoid light scattering[1,17–19,26], which realizes high-resolution three-dimensional printing by micro-stereolithography[1]; and adding light absorbers and/or radical inhibitors to optimize the printing resolution[2,3,9,17,24]. Based on these techniques, various ceramic/glass (SiO_2[1,9,17–22], Al_2O_3[3,10,11,15,16,21], ZrO_2[4,5,12], Si_3N_4[8], $Ca_3(PO_4)_2$[2,3], $Pb(Zr,Ti)O_3$[14], $BaTiO_3$[25], wollastonite ($CaO·SiO_2$)[6], diopside ($CaO·MgO·2SiO_2$)[6], and $Ca_{10}(PO_4)_6(OH)_2$[7]) parts with complex structures have been successfully prepared through additive manufacturing and/or molding with these designed photo-curable suspensions. However, all systems undergo very slow and complex-programmed debinding/sintering (Supplementary Fig. 1) to avoid crack formation/structural collapse due to rapid gas generation caused by large content of monomers in the suspension. For instance, debinding and sintering of SiO_2 green parts fabricated from conventional photo-curable SiO_2 suspensions can take up to 48 h[1,9,17,19,22], which is unfavorable to improve the manufacturing efficiency. As well as photo-curable suspensions, the usage of photo-curable preceramic polymers is also an effective route for three-dimensional structuring of ceramic/glass parts. Various pre-ceramic polymers, such as based on polysiloxanes[27–29], polycarbosilanes[30], polycarbosilazanes[31], and metal alkoxides complexed with acrylic acids[32] have printed through stereolithographic process as well, and successfully pyrolysed to form $SiOC$[27,28], SiO_2[29], SiC[30], $SiCN$[31], and $ZrOC$[32] components. Recent study also showed that three-dimensionally structured, nanoporous, and multicomponent transparent glass can be printed using multicomponent pre-ceramic polymers which were designed to induce phase separations during photo-polymerization[33]. However, three-dimensional structuring based on polymer derived ceramic process also suffer from slow heating profiles (heating rates typically reported to be 0.4–2.0 °C min^{-1}) for pyrolysis.

Here, we propose a new concept for preparing a photo-curable suspension that only requires small amounts of organic additives to enable rapid debinding and sintering of the obtained photo-cured green compacts. Completely different from the conventional process which involves polymerization of monomers used as a solvent/matrix, the proposed process is designed to have photo-initiated interparticle network formation reaction by small amount of monomers in well stabilized non-aqueous suspensions (Fig. 1a). The manufacturing process of transparent SiO_2 glass from SiO_2 suspensions is selected as a model system to prove our concept. In addition to reducing the organic content in the photo-curable suspension, the proposed suspension system is also designed to simultaneously achieve improved suspension

transparency and a highly dispersed state of particles under concentrated conditions to realize the applicability of the suspension to shaping processes in a wide range of scales (from micro-scale stereolithography to centimeter-scale in-situ solidification) and to achieve densified transparent SiO_2 glass after atmospheric pressure sintering of the green compacts.

Briefly, SiO_2 fine particles are dispersed in a mixed solvent of α-terpineol and tetrahydrofuran (THF) with assistance from polyethyleneimine partially complexed with oleic acid (PEI-OA). PEI-OA is designed to serve as a universal functional polymer dispersant that could be attached onto various series of particles[34–37]. The content of OA segment in PEI-OA is varied to tune the dispersion stability of SiO_2 fine particles in the solvent while the remaining un-complexed amino groups in PEI-OA were expected to act as cross-linking reaction sites. The ratio of α-terpineol and tetrahydrofuran (THF) is also varied so as to match the refractive index of the solvent with that of the SiO_2 fine particles for improving the transparency of the suspension. Then, the photo-radical initiators and a small amount of multifunctional acrylates (MA, only 5 wt%, based on SiO_2 particles) are dissolved into the prepared suspension. By UV light irradiation on this suspension, we expect MA to be polymerized by an exothermic reaction. Further, the generated polymerization heat will aid the Michael additive reaction between the polymerized MA and the residual amine groups of PEI-OA on the SiO_2 fine particles, thereby resulting in site-selective suspension solidification by inter-particle network formation. We will demonstrate that the proposed photo-curable suspension can be applied to various shaping processes, including micro-scale stereolithography and centimeter-scale in-situ solidification, and can be further processed into transparent SiO_2 glass materials through rapid debinding/sintering even under non-vacuumed atmospheric conditions. The total duration time of debinding/sintering profiles will be reduced at least half a day (at least 77% reduction in time) compared to the case of SiO_2 green compacts prepared by conventional photo-curable suspensions (Supplementary Fig. 1b).

Results and discussion

Design of interparticle photo-cross-linkable suspensions. The visual appearances of the designed photo-curable suspensions with different mixing volume ratios of α-terpineol: THF and their in-line transmittances are shown in Fig. 1b and Supplementary Fig. 2, respectively. In these figures, the mono-solvent suspensions (α-terpineol: THF = 100:0 and 0:100) exhibit strong turbidity, whereas the mixed-solvent suspensions of α-terpineol and THF exhibit improved in-line transmittances. It is demonstrated that the matching of refractive indices (n) of the mixed solvent ($n_{α-terpineol} = 1.4831$ ($λ = 589.3$ nm, $T = 293.15$ K)[38], $n_{THF} = 1.4070$ ($λ = 589.3$ nm, $T = 293.15$ K)[39]) with that of the SiO_2 particles ($n_{SiO2} = 1.4584$ ($λ = 589.3$ nm, $T = 293.15$ K)[40]) reduces the light scattering in the suspension. With respect to the wavelength region (365, 405 nm) that is used for shaping in this study, an α-terpineol: THF mixing ratio of 55:45 was found to be optimal to increase the in-line transmittance of the suspension (Supplementary Fig. 2). Figures 1c and d presents the effect of UV (365 nm) energy dose on the curing depth of the designed suspension and visual examples of the photo-cured suspension, respectively. The curing depth was analyzed by a molding based macroscopic method which UV light was irradiated from the bottom of the glass tube filled with the suspension. The designed suspension was photo-curable even when the additive content of the photo-responsive monomers is extremely low (only 4.5–23 % compared to previous reports[1,9,17–19,21]). The increase in the transparency of the suspension by control of the solvent
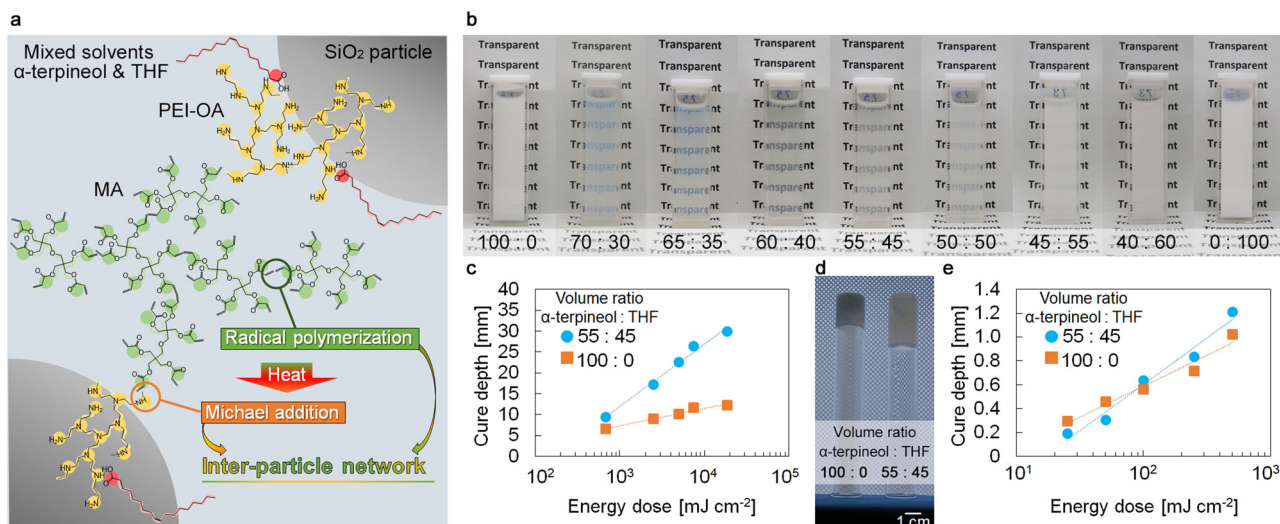
Fig. 1 Design of transparent photo-curable SiO₂ suspensions with suppressed organic additives. a Schematic illustration for the concept of the photo-curable suspension design. **b** Visual appearance of the SiO₂ suspension (42 vol%) with various mixing volume ratios of α-terpineol to THF. **c** Cure depth of photo-curable SiO₂ suspension characterized by a molding based macroscopic approach. **d** Photo-cured suspension after UV irradiation (18,420 mJ cm^{-2}). **e** Cure depth of photo-curable SiO₂ suspension characterized by a stereo-lithography based microscopic approach.

composition successfully increased the curing depth in centimeter region, which will be favorable to photo-cure relatively large (centimeter-scale) components. On the other hand, Fig. 1e shows the effect of UV (405 nm) energy dose on the micro-scaled curing depth of the designed suspension which was characterized using the laser-based stereolithographic apparatus. Smaller curing depths were achieved at lower energy dose conditions when the transparency of the suspension was increased. This is because of the reduction of light scattering in the transparent suspension, which will be favorable to photo-cure micro-meter scale components.

To understand the dispersion stability and photo-curing behavior of the designed suspension, the effects of the particle concentrations and the OA content in PEI-OA on the suspension flow curves and storage modulus (G′) are shown in Fig. 2a–d. The suspension designed using PEI-OA (15 mol% OA in PEI-OA) exhibits flow curves without hysteresis during increasing and decreasing shear rates (Fig. 2a) even under higher particle concentrations (~42 vol%). This indicates that no strong aggregates collapsible by shear were present, and that the suspension was well-stabilized before UV light irradiation. The content of OA in PEI-OA also affected the flow curves of the suspension (Fig. 2b); although no strong aggregates were present (i.e., no strong hysteresis properties were found in the flow curves), the suspension viscosity gradually increased with increasing OA content in PEI-OA. The surface affinity between the particle surface and the α-terpineol/THF mixed solvent was presumed to have been reduced with increasing OA content in PEI-OA.

The real-time photo-curing properties of these well-dispersed suspensions with different particle concentrations and OA contents in PEI-OA were further characterized by monitoring the changes in G′ using a rheometer under UV irradiation. For all cases, a remarkable increase in G′ was observed just after UV light irradiation. Interestingly, the changes in G′ before and after UV irradiation became greater and the response time of G′ was shortened with increasing particle concentration in the suspensions (Fig. 2c). Furthermore, the solidification behavior was suppressed with increasing OA content in PEI-OA (Fig. 2d).

To understand the changes in the surface structures of SiO₂ particles by UV light irradiation, SiO₂ particles before and after

UV light irradiation (after 15 s and 30 s) were collected from the suspension and analyzed by FTIR and TGA after washing using THF to detach unreacted molecules from the particles. From the FTIR spectra shown in Fig. 2e, signals attributed to vibrations of the interior siloxane bonds (1866 cm^{-1})[41] and OH bending vibrations (1630 cm^{-1}) of the surface-bound water[41] were found in the raw powder sample. For the SiO₂ particles before UV irradiation, bands correspond to CH₂ scissoring (1462 cm^{-1}) were further detected, which originated from OA[42-44] and PEI[45]. A small absorbance of the C=O stretching vibration (1732 cm^{-1}) from MA[46] was also detected, suggesting the occurrence of the Michael additive reaction between MA and amino groups of PEI-OA bound on the particle surface, at room temperature in slight degree. A small weight loss was observed in the TGA curves from SiO₂ particles collected before UV irradiation, which further supports the presence of PEI-OA and a small amount of MA (Fig. 2f). After UV irradiation, bands related to the C=O stretching vibration (1732 cm^{-1}) and –CH=CH₂ scissoring (1406 cm^{-1})[47] originating from MA significantly increased in the FTIR spectra. Furthermore, increased weight loss was detected in the TGA with increasing UV irradiation time. These results suggest that larger amounts of MA have fixed on the PEI-OA-modified SiO₂ particle surface by the UV light-induced photo-polymerization of MA and the Michael additive reaction between polymerized MA and amino groups of PEI-OA bound on particle surface. Considering that suspension temperature rapidly increased during UV light irradiation when MA was in presence (Supplementary Methods, Supplementary Fig. 3), it can be suggested that MA polymerization heat was generated and aided the Michael additive reaction. Owing to network formation among the PEI-OA-modified SiO₂ particles by polymerized MA, fibrous polymer-like networks were found in the fractured surface of the solidified suspension (Fig. 2g). Since only bulky polymers were identified among SiO₂ particles when UV light was irradiated on the suspension prepared without fixing PEI-OA on the SiO₂ particle surface (Fig. 2h), the presence of PEI-OA on the particle surface as the reaction site with polymerized MA through the Michael additive reaction was key to achieving effective photo-responsivity. Based on the above-mentioned findings, the increase in the solidification degree and shortening of solidification response time with increasing particle

3
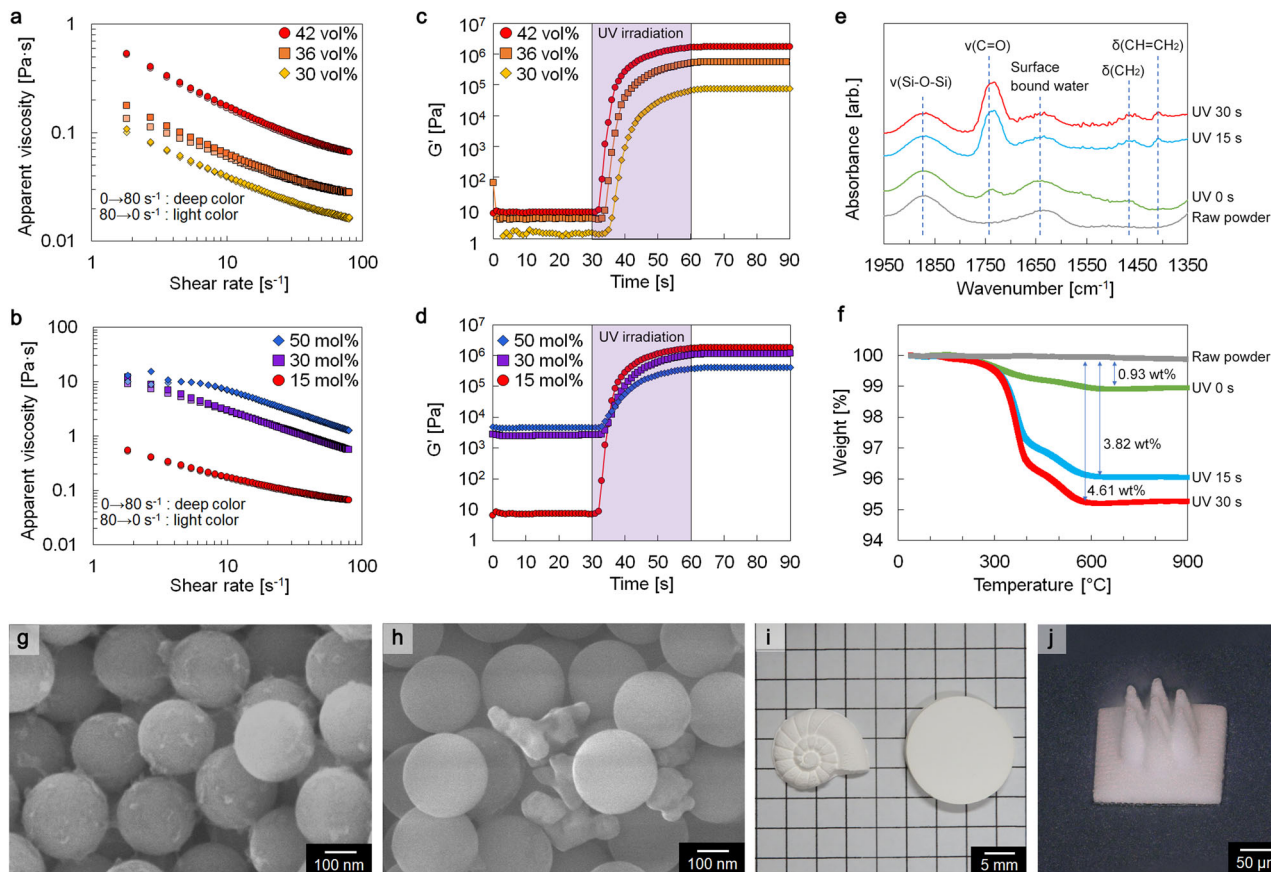
Fig. 2 Photo-curing behaviors of SiO$_2$ suspensions. a Flow curves of SiO$_2$ suspensions (before UV irradiation) with different SiO$_2$ concentrations (MA content: 5 wt%, 15 mol% OA in PEI-OA) and **b** different OA contents in PEI-OA (MA content: 5 wt%, SiO$_2$ concentration: 42 vol%). **c** Storage modulus under UV irradiation of SiO$_2$ suspensions with different SiO$_2$ concentrations (MA content: 5 wt%, 15 mol% OA in PEI-OA) and **d** different OA contents in PEI-OA (MA content: 5 wt%, SiO$_2$ concentration: 42 vol%). **e** FT-IR spectra and **f** TGA profiles of SiO$_2$ particles collected before and after UV irradiation. **g** SEM images of fracture surface of green compacts with and **h** without addition of PEI-OA. **i** Photo-cured green compacts obtained through in-situ solidification and **j** micro-scale stereolithography.

concentration (Fig. 2c) can be explained by the effective inter-particle network formation realized by the decrease in the inter-particle surface distances. Furthermore, the suppression of solidification behavior with increasing OA content (Fig. 2d) can be explained by the reduction of the remaining amino groups in PEI-OA, which was a reaction site for network formation with the polymerized MA.

Three-dimensional structuring of transparent SiO$_2$ glass. Using the 42 vol% SiO$_2$ suspension stabilized with PEI-OA containing 15 mol% OA in a mixed solvent of THF and α-terpineol as the standard photo-curable suspension, our newly designed photo-curable suspensions could be applied toward shaping centimeter-scaled green compacts by photo-curing in a mold (Fig. 2i), as well as toward micro-meter-scaled stereo-lithography (Fig. 2j). Owing to the formation of the photo-induced polymer network among the particles, 1.28% linear shrinkage was observed during photo-curing in a disk-shaped mold. Furthermore, the photo-cured green compacts could be dried without inducing collapse and cracking by simply leaving the sample in a 100 °C oven (for at least 180 min, Supplementary Fig. 4). This process was considerably rapid compared to drying during the general in-situ solidification[48–51], that required more than 12 h. In addition, the strength of the dried green compact with a network-like inter-particle cross-linked polymer was 2.04 MPa, while that of the green compact without PEI-OA was 0.25 MPa (Supplementary Methods, Supplementary Fig. 5).

The effects of MA contents in the photo-responsive suspensions and the heating rates of the corresponding photo-cured compacts on the appearance of the sintered material are shown in Fig. 3a. The size of the photo-cured green compacts before sintering was 20 mm in diameter and 3.9 mm in thickness. The MA content was varied between 5 and 20 wt% to the particles, which is low compared to the monomer content in conventional photo-responsive suspensions. From TGA analysis, overall weight loss from the green compact to the sintered material, including PEI-OA, were 7 wt%, 12 wt%, and 24 wt% to the particles when MA content was 5 wt%, 10 wt%, and 20 wt% to the particles, respectively (Supplementary Fig. 6). Note also that the heating rate was varied from 5 to 20 °C min^{-1}, which is higher than that in existing additive manufacturing/in-situ solidification (c.a. 0.1 to 1.6 °C min^{-1})[1–4,9–13,15–19,25] using photo-curable suspension. When the heating rate was 5 °C min^{-1}, transparent (Fig. 3b) and densified (2.19 g cm^{-3} by the Archimedes method) sintered SiO$_2$ glass was successfully obtained, without forming crystal phases (Fig. 3c), even when sintering the green compacts at ambient pressure for all MA additive conditions. Considering the full density of fused silica glass (2.20 g cm^{-3}), there might be slight number of defects remained in the sintered materials which can be improved by vacuum sintering. The overall linear shrinkage after sintering were 24.7% in width and in height. The three-point bending strength and the Vickers hardness was 84 MPa (SD 11) and 9.66 GPa (SD 0.70), respectively ($n = 10$, Supplementary Fig. 7). Owing to the realization of highly particle-packed
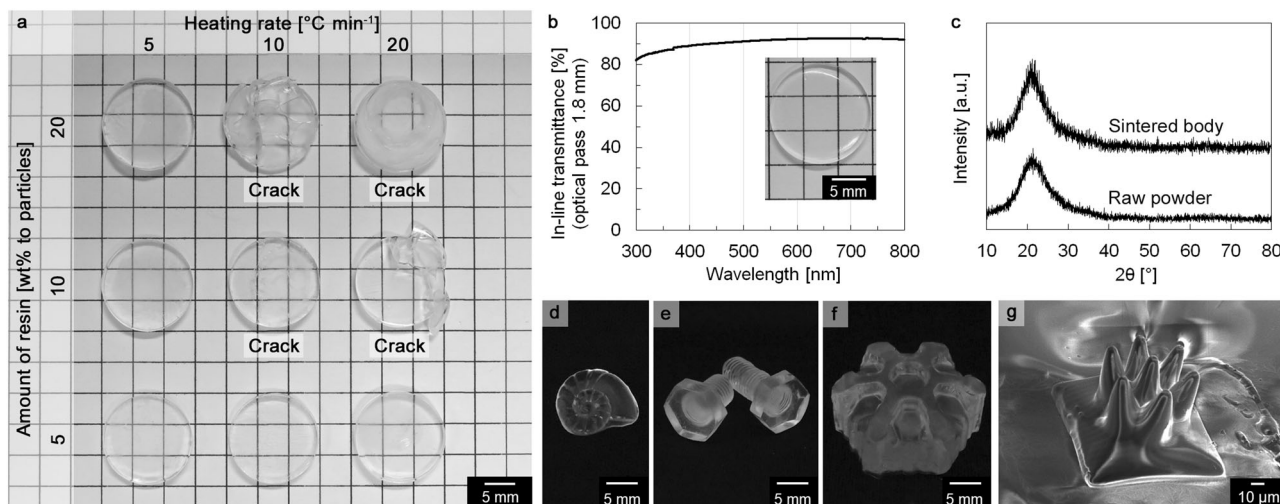
Fig. 3 Debinding and sintering of photo-cured SiO₂ green compacts. a Sintered SiO₂ glass prepared from photo-curable suspensions with different MA contents and heating rates. **b** In-line transmittance and **c** XRD patterns of sintered glass (5 wt% MA content in photo-curable suspension, heating rate: 5 °C min⁻¹). Sintered SiO₂ glass from green components prepared through **d–f** in-situ solidification and **g** stereolithography using photo-curable SiO₂ suspensions (MA content: 5 wt%, heating rate: 5 °C min⁻¹).

photo-cured green compacts from the concentrated and non-aggregated suspensions, transparent sintered SiO₂ glass was obtained without employing vacuum sintering conditions. With increasing heating rates, cracks began to form for the green compacts prepared using photo-responsive suspensions containing higher contents of MA (10 wt% and 20 wt%). On the other hand, by reducing the MA additive content to 5 wt%, which was still enough to induce photo-responsive properties in the suspension (Fig. 2), a transparent sintered SiO₂ glass material was obtained even at increased heating rates. Owing to the rapid dryable, debindable, and sinterable properties of the photo-cured green compacts prepared from our newly proposed photo-responsive suspensions, the overall processing time for drying/debinding/sintering of photo-cured green compacts can be shortened to a significant extent (Supplementary Fig. 1), which should be industrially friendly and energy conserving. Here, we should note that the thickness of the photo-cured green compacts may affect to the time needed for thermal-debinding process. However, as demonstrated in Fig. 3d–g, even the green compacts photo-cured using centimeter-scaled complex-structured molds (for instance, the green compact corresponds to Fig. 3f had the side length of 22 mm in the hexagonal structure and the thickness of 12–16 mm) as well as micro-scaled green compacts fabricated through stereo-lithography can also be sintered into transparent glass components through the rapid heating profiles. We would like to note also that, similarly to the previous reports[1,9], the glass components can simply be functionalized by metal ions in our proposed photo-responsive suspensions. For instance, a photo-responsive suspension can be designed using PEI-OA partially complexed with metal ions such as Cu, Eu, and Ce (0.19, 0.15, and 0.15 mol%, based on the number of PEI monomer units, respectively. See Supplementary Methods for the detailed procedures.). The sintered transparent SiO₂ glass component fabricated from this photo-responsive suspension with metal-doped PEI-OA exhibited photoluminescence (Fig. 4a–c). By virtue of the realization of rapid dryable/debindable/sinterable green compacts from photo-responsive suspensions to form complex-structured transparent glass materials, we believe that the proposed photo-responsive suspension system will offer novel opportunities for the design of industry-friendly and energy/time-saving ceramic/glass fabrication processes through additive manufacturing/molding techniques.
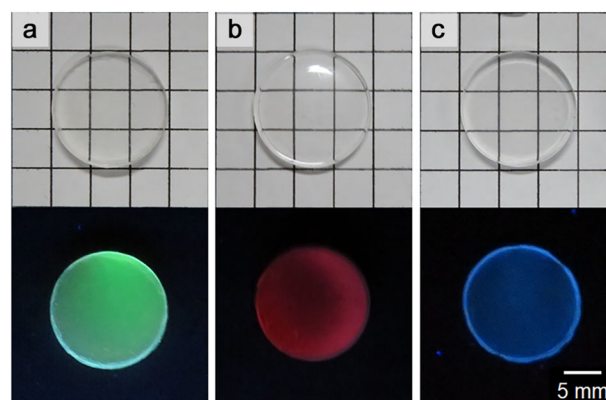
Fig. 4 Demonstration of glass functionalization. Photographs of luminescent glass doped with **a** Cu, **b** Eu, and **c** Ce metal ions captured under room light and a UV lamp (365 nm for (**a**) and (**b**), 254 nm for (**c**)).

In summary, the design of a highly dispersed photo-responsive SiO₂ suspension that could be cured using a suppressed amount of multifunctional acrylates was demonstrated by dispersing PEI-OA-modified SiO₂ particles into a mixed solvent of α-terpineol and THF with photo-radical initiators and MAs. UV light irradiation on the suspension resulted in successful photo-curing by polymer network formation among SiO₂ particles, which occurred due to the photo-polymerization of MA and the Michael additive reaction between the polymerized MA and amino groups of PEI-OA on SiO₂ particles. Tuning of the α-terpineol/THF ratio was effective in controlling the refractive index matching between the solvent and SiO₂ particles. This was beneficial to suppress the light scattering in the suspension and to increase the curing depth. The suspension could be employed in various shaping process such as micro-scale stereolithography to centimeter-scale in-situ solidification even the additive content of the photo-responsive monomers was extremely low. Owing to the limited amount of monomers in the suspension, the complex-structured SiO₂ green compacts were processable into transparent glass components through rapid debinding and sintering, which the heating profiles were reduced at least 14 h (77% reduction in

time) compared to the case of conventionally photo-cured SiO$_2$ green compacts.

Methods

Materials. Polyethyleneimine (PEI, average molecular weight 1800), oleic acid (OA), and tetrahydrofuran (THF, 99.5%) were purchased from FUJIFILM Wako Pure Chemical Co., Ltd., Japan. α-Terpineol (80.0%), 2,2-dimethoxy-2-phenyla-cetophenone (DPA) as a radical initiator for in-situ solidification and 2-(5-chloro-2-benzotriazolyl)-6-tert-butyl-p-cresol as an UV absorber were purchased from Tokyo Chemical Industry Co., Ltd., Japan. Diphenyl (2,4,6-trimethylbenzoyl) phosphine oxide as a radical initiator for stereolithography was purchased from Merck KGaA, Germany. Multifunctional acrylate (MA, a mixture of di-pentaerythritol pentaacrylate (40–50%) and di-pentaerythritol hexaacrylate) was a gift from Toagosei Co., Ltd., Japan. SiO$_2$ nanoparticles (KE-S30, 12.6 m^2 g^{-1} analyzed by BET) were purchased from Nippon Shokubai Co., Ltd., Japan.

Preparation of photo-responsive suspension. First, PEI–OA complexes with different OA contents (15–50 mol% of OA in PEI monomer units, calculated assuming all amines were secondary amines) in PEI were prepared in a manner similar to that in our previous report[34–37]. Briefly, 0.500 g of PEI and 0.493, 0.986, and 1.642 g of OA, corresponding to 15, 30, and 50 mol% OA, respectively, were mixed with α-terpineol to prepare a 10.0 g solution. The obtained solutions were treated in an ultrasonic bath for 5 min, and then magnetically stirred for 24 h. The respective PEI-OA were then dissolved into various mixed solutions of α-terpineol and THF (THF contents: 0, 30, 35, 40, 45, 50, 55, 60, and 100 vol%). SiO$_2$ fine particles (42 vol%) and ZrO$_2$ balls (φ 5 mm, volume fraction of the suspension: balls = 100:32) were added into the as-prepared solution. Planetary mixing with a THINKY ARE-250 mixer (500 rpm, 5 min) was followed by ball-milling (160 rpm) for 24 h. The additive contents of PEI-OA at 15, 30, and 50 mol% OA were controlled to be 1.0 mg m^{-2}, 1.3 mg m^{-2}, and 2.0 mg m^{-2}, respectively, based on the total SiO$_2$ surface area in the suspensions. These additive contents were pre-determined to ensure their saturated adsorbed content on SiO$_2$ particles (Supplementary Methods, Supplementary Fig. 8). After ball-milling for 24 h, MA (5 wt.% to particles) and the photo-radical initiator (2 wt% to MA) were added to the suspensions and further mixed by a planetary mixer (2000 rpm, 3 min). Finally, the photo-responsive suspensions were obtained by de-gassing the suspension through centrifugation (2200 rpm, 2 min) after removing the balls.

Shaping, debinding, and sintering of the SiO$_2$ green parts. SiO$_2$ green parts were shaped from the photo-curable suspension via in-situ solidification in silicone molds and by stereo-lithography. For the in-situ solidification, the photo-curable suspension was poured into a centimeter-scale silicone mold having various structures (maximum depth: 21 mm), and irradiated with UV light of wavelength 365 nm. SiO$_2$ green parts were obtained by demolding the photo-cured SiO$_2$ suspension, and subsequently dried at 80 °C or 100 °C. Three-dimensional micro-fabrication with laser-based stereo-lithography was carried out using the in-house built apparatus reported before[52] with 405 nm laser. Over-curing along the z-axis was prevented using the absorber 2-(5-chloro-2-benzotriazolyl)-6-tert-butyl-p-cresol. After shaping a set of seven axial cones (laser intensity: 60 mW, scan speed: 130 μm s^{-1}, layer thickness: 10 μm), the modeled objects were gently washed with toluene and further dried at 80 °C. For debinding and sintering, the dried green parts were simply heated to 1350 °C at a heating rate of 5–20 °C min^{-1} and held there for 30 min under atmospheric conditions using an electric furnace (M-1700, Watanabe Manufacturing Co., Ltd., Japan).

Characterizations. The in-line transmittance of the photo-responsive suspension with different THF: α-terpineol ratios was characterized using a UV–vis spectro-photometer (V-630, JASCO Co., Ltd., Japan). The cure depths of the suspensions were characterized by a molding based macroscopic approach and stereo-lithography based microscopic approach. For the former case, the photo-responsive suspensions were poured in a glass tube (φ15.8 mm) and 365 nm UV light (670–18,420 mJ cm^{-2}) was irradiated from the bottom. After decanting the un-cured suspension, the height of the residual solidified suspension in the tube was measured. For the latter case, the photo-responsive suspensions were poured on a glass substrate and 405 nm UV light (25–500 mJ cm^{-2}) was irradiated from the bottom using stereo-lithographic apparatus. After rinsing the solidified object by toluene, the height of solidified product was measured by an optical microscope (VHX-5000, KEYENCE, Japan). Using a rheometer (MCR102, Anton Paar Japan Industry Co., Ltd., Japan), we characterized the flow curves and changes in the storage modulus under UV irradiation. For the flow curves, the shear stress was monitored with increasing shear rate from 0 to 80 s^{-1} in 90 s and decreasing shear rate from 80 to 0 s^{-1} in 90 s using a cone-plate apparatus at 25 °C. The change in the storage modulus was measured using a cone-transparent glass plate apparatus under a strain of 0.1% and a frequency of 1.0 Hz. UV light of wavelength 365 nm was irradiated (83 mW cm^{-2}) for 30–60 s from the bottom of the glass plate after starting the measurement. Fourier-transform infrared (FT-IR) spectroscopy (FT/IR-6000, JASCO CO., Ltd., Japan) and thermogravimetric analysis (TGA) (Thermo Plus EVO, RIGAKU CO., Ltd., Japan) were conducted to characterize the structure of the particle surface before and after UV irradiation. The powder samples for

FT-IR and TGA analyses were prepared by centrifuging the suspension, washing the sediment with THF, and drying at 80 °C. The fractured surface of photo-cured green body was characterized by field emission-scanning electron microscope (FE-SEM, SU8010, Hitachi High-Technologies, Co., Japan). The relative density of the sintered body was measured by the Archimedes method. X-ray diffraction (XRD, RINT 2000, Rigaku Co., Japan) was conducted (40 kV, 20 mA, CuKα, 2.0° min^{-1}.) to verify that the crystallization of the amorphous phase, which causes devi-trification, was not promoted during sintering. A UV–vis spectrophotometer was used to characterize the optical transmission spectra of the sintered body without conducting any surface polishing. Vickers hardness was measured by a hardness tester (AVK-C1, Akashi, Japan). The applied load was 9.80 N and the loading time was 15 s. Three-point bending strength was measured by a universal testing machine (AG-X 50kN, Shimadzu Co., Japan) using a specimen having the size of 18 mm × 2 mm × 1.4 mm.

Data availability

The data supporting the findings of this study are available from the corresponding authors upon request.

References

1. Kotz, F. et al. Three-dimensional printing of transparent fused silica glass. *Nature* **544**, 337–339 (2017).
2. Pfaffinger, M., Hartmann, M., Schwentenwein, M. & Stampfl, J. Stabilization of tricalcium phosphate slurries against sedimentation for stereolithographic additive manufacturing and influence on the final mechanical properties. *Int. J. Appl. Ceram. Technol.* **14**, 499–506 (2017).
3. Felzmann, R. et al. Lithography-based additive manufacturing of cellular ceramic structures. *Adv. Eng. Mater.* **14**, 1052–1058 (2012).
4. He, R. et al. Fabrication of complex-shaped zirconia ceramic parts via a DLP-stereolithography-based 3D printing method. *Ceram. Int.* **44**, 3412–3416 (2018).
5. Wang, J.-C. & Dommati, H. Fabrication of zirconia ceramic parts by using solvent-based slurry stereolithography and sintering. *Int. J. Adv. Manuf. Technol.* **98**, 1537–1546 (2018).
6. Schmidt, J., Elsayed, H., Bermardo, E. & Colombo, P. Digital light processing of wollastonite-diopside glass-ceramic complex structures. *J. Eur. Ceram. Soc.* **38**, 4580–4584 (2018).
7. Zeng, Y. et al. 3D printing of hydroxyapatite scaffolds with good mechanical and biocompatible properties by digital light processing. *J. Mater. Sci.* **53**, 6291–6301 (2018).
8. Huang, R.-J. et al. Fabrication of complex shaped ceramic parts with surface-oxidized Si$_3$N$_4$ powder via digital light processing based stereolithography method. *Ceram. Int.* **45**, 5158–5162 (2019).
9. Liu, C., Qian, B., Liu, X., Tong, L. & Qiu, J. Additive manufacturing of silica glass using laser stereolithography with a top-down approach and fast debinding. *RSC. Adv* **8**, 16344–16348 (2018).
10. Zhou, M. et al. Preparation of a defect-free alumina cutting tool via additive manufacturing based on stereolithography—optimization of the drying and debinding processes. *Ceram. Int.* **42**, 11598–11602 (2016).
11. An, D. et al. Additive manufacturing and characterization of complex Al$_2$O$_3$ parts based on a novel stereolithography method. *Int. J. Appl. Ceram. Technol.* **14**, 836–844 (2017).
12. Lian, Q. et al. Accurate printing of a zirconia molar crown bridge using three-part auxiliary supports and ceramic mask projection stereolithography. *Ceram. Int.* **45**, 18814–18822 (2019).
13. Provin, C., Monneret, S., Gall, H. L. & Corbel, S. Three-dimensional ceramic microcomponents made using microstereolithography. *Adv. Mater.* **15**, 994–997 (2003).
14. Yang, Y. et al. Three-dimensional printing of high dielectric capacitor using projection based stereolithography method. *Nano Energy* **22**, 414–421 (2016).
15. He, L., Fei, F., Wang, W. & Song, X. Support-free ceramic stereolithography of complex overhanging structures based on an elasto-viscoplastic suspension feedstock. *ACS Appl. Mater. Interfaces* **11**, 18849–18857 (2019).
16. Hazan, Y., de., Thänert, M., Trunec, M. & Misak, J. Robotic deposition of 3d nanocomposite and ceramic fiber architectures via UV curable colloidal inks. *J. Eur. Ceram. Soc.* **32**, 1187–1198 (2012).
17. Wozniak, M., Graule, T., Hazan, Y., de., Kata, D. & Lis, J. Highly loaded UV curable nanosilica dispersions for rapid prototyping applications. *J. Eur. Ceram. Soc.* **29**, 2259–2265 (2009).
18. Kotz, F. et al. Liquid glass: a facile soft replication method for structuring glass. *Adv. Mater.* **28**, 4646–4650 (2016).

19. Kotz, F. et al. Glassomer—processing fused silica glass like a polymer. *Adv. Mater.* **30**, 1–5 (2018).
20. Kotz, F. et al. Fabrication of arbitrary three-dimensional suspended hollow microstructures in transparent fused silica glass. *Nat. Commun.* **10**, 1439 (2019).
21. Hazan, Y., de., Wozniak, M., Heinecke, J., Müller, G. & Graule, T. New microshaping concepts for ceramic/polymer nanocomposite and nanoceramic fibers. *J. Am. Ceram. Soc* **93**, 2456–2459 (2010).
22. Shepherd, R. F. et al. Stop-flow lithography of colloidal, glass, and silicon microcomponents. *Adv. Mater.* **20**, 4734–4739 (2010).
23. Brady, G. A. & Halloran, J. W. Differential photo-calorimetry of photopolymerizable ceramic suspensions. *J. Mater. Sci.* **33**, 4551–4560 (1998).
24. Tomeckova, V. & Halloran, J. Cure depth for photopolymerization of ceramic suspensions. *J. Eur. Ceram. Soc.* **30**, 3023–3033 (2010).
25. Chen, Z. et al. 3D printing of piezoelectric element for energy focusing and ultrasonic sensing. *Nano Energy* **27**, 78–86 (2016).
26. Aloui, F., Lecamp, L., Lebaudy, P. & Brurel, F. Relationships between refractive index change and light scattering during photopolymerization of acrylic composite formulations. *J. Eur. Ceram. Soc.* **36**, 1805–1809 (2016).
27. Zanchetta, E. et al. Stereolithography of SiOC ceramic microcomponents. *Adv. Mater.* **28**, 370–376 (2016).
28. Eckel, Z. C. et al. Additive manufacturing of polymer-derived ceramics. *Science* **351**, 58–62 (2016).
29. Cooperstein, I. et al. Additive manufacturing of transparent silica glass from solutions. *ACS Appl. Mater. Interfaces* **10**, 18879–18885 (2018).
30. Hazan, Yde & Penner, D. SiC and SiOC ceramic articles produced by stereolithography of acrylate modified polycarbosilane systems. *J. Eur. Ceram. Soc.* **37**, 5205–5212 (2017).
31. Pham, T. A. et al. Three-dimensional SiCN ceramic microstructures via nano-stereolithography of inorganic polymer photoresists. *Adv. Func. Mater* **16**, 1235–1241 (2006).
32. Fu, Y. et al. Preparation and stereolithography 3D printing of ultralight and ultrastrong ZrOC porous ceramics. *J. Alloys Compd.* **789**, 867–873 (2019).
33. Moore, D. G., Barbera, L., Masania, K. & Studart, A. R. Three-dimensional printing of multicomponent glasses using phase-separating resins. *Nat. Mater.* **19**, 212–217 (2020).
34. Iijima, M., Okamura, N. & Tatami, J. Polyethyleneimine–oleic acid complex as a polymeric dispersant for Si₃N₄ and Si₃N₄-based multicomponent nonaqueous slurries. *Ind. Eng. Chem. Res.* **54**, 12847–12854 (2015).
35. Iijima, M., Kawaharada, Y. & Tatami, J. Effect of fatty acids complexed with polyethyleneimine on the flow curves of TiO₂ nanoparticle/toluene suspensions. *J. Asian Ceram. Soc.* **4**, 277–281 (2016).
36. Morita, S., Iijima, M. & Tatami, J. SiO₂ nanoparticles surface modified with polyethyleneimine-oleic acid complex as stabilizers of Ni fine particles in dense nonaqueous suspensions. *Adv. Powder Technol.* **28**, 30–36 (2017).
37. Iijima, M., Okamura, N. & Tatami, J. Effect of polyethyleneimine-fatty acid complex type dispersant structure on the overall processing chain of Si₃N₄ ceramics using multicomponent non-aqueous slurries. *Adv. Powder Technol.* **29**, 3440–3447 (2018).
38. NPCS Board of Consultants & Engineers. *Industrial Alcohol Technology Handbook* (Asia Pacific Business Press Inc., Delhi, 2010).
39. Knežević-Stevanovic, A. B., Šerbanovic, S. P., Radovic, I. R., Djordjevic, B. D. & Kijevčanin, M. L. Thermodynamic and spectroscopic study of the ternary system dimethyladipate + tetrahydrofuran + 1-butanol at T = (288.15 to 323.15) K. *J. Chem. Eng. Data* **58**, 2932–2951 (2013).
40. Malitson, I. H. Interspecimen comparison of the refractive index of fused silica. *J. Opt. Soc. Am.* **55**, 1205–1208 (1965).
41. Feldmann, V., Engelmann, J., Gottschalk, S. & Mayer, H. A. Synthesis, characterization and examination of Gd[DO3A-hexylamine]-functionalized silica nanoparticles as contrast agent for MRI-applications. *J. Colloid Interface Sci.* **366**, 70–79 (2012).
42. Tandon, P., Raudenkolb, S., Neubert, R. H. H., Rettig, W. & Wartewig, S. X-ray diffraction and spectroscopic studies of oleic acid–sodium oleate. *Chem. Phys. Lipids.* **109**, 37–45 (2001).
43. Palma., R. D. et al. Silane ligand exchange to make hydrophobic superparamagnetic nanoparticles water-dispersible. *Chem. Mater.* **19**, 1821–1831 (2007).
44. Kadamne, J. V., Jain, V. P., Saleh, M. & Proctor, A. Measurement of conjugated linoleic acid (CLA) in CLA-rich soy oil by attenuated total reflectance-Fourier transform infrared spectroscopy (ATR-FTIR). *J. Agric. Food Chem.* **57**, 10483–10488 (2009).
45. Iijima, M., Sato, K., Kurashima, K., Ishigaki, T. & Kamiya, H. Low-temperature synthesis of redispersible iron oxide nanoparticles under atmospheric pressure and ultradense reagent concentration. *Powder Technol.* **181**, 45–50 (2008).
46. Wen, J. et al. UV-curable hydrophobic coatings of functionalized carbon microspheres with good mechanical properties and corrosion resistance. *Coatings* **8**, 439 (2018).
47. Bach, M. *Near Infrared Laser Sensor System for In-Line Detection of Conversion in UV-Cured Polymer Coatings.* (KIT Scientific Publishing, Karlsruhe, 2014).
48. Hu, Y., Zhongjian, W. & Jianying., L. Study on the gel casting of fused silica glass. *J. Non-Cryst. Solids.* **354**, 1285–1289 (2008).
49. Chen, A.-N. et al. Rapid in-situ solidification of SiO₂ suspension by direct coagulation casting via controlled release of high valence counter ions from calcium iodate and pH shift. *Ceram. Int.* **43**, 1930–1936 (2017).
50. Ikeda, H., Murata, T. & Fujino, S. Fabrication and photoluminescence of monolithic silica glass doped with alumina nanoparticles using SiO₂-PVA nanocomposite. *J. Eur. Ceram. Soc.* **123**, 550–553 (2015).
51. Jia, Y., Kanno, Y. & Xie, Z. New gel-casting process for alumina ceramics based on gelation of alginate. *J. Eur. Ceram. Soc.* **22**, 1911–1916 (2002).
52. Maruo, S. & Ikuta, K. Three-dimensional microfabrication by use of single-photon-absorbed polymerization. *Appl. Phys. Lett.* **76**, 2656–2658 (2000).

Acknowledgements

Author contributions

M.I. conceived this project. R.A. and S. Morita performed the suspension preparation, in-situ solidification, and their analysis. Y.F., T.F., and S. Maruo performed the 3D printing by stereolithograpy. R.A. and J.T. performed the sintering and the characterization of sintered material. R.A. and M.I. cowrote the draft of this paper. All authors discussed the results and commented on the paper.

Competing interests

The authors declare no competing interests.

Additional information

Supplementary information is available for this paper at https://doi.org/10.1038/s43246-020-0029-y.

Correspondence and requests for materials should be addressed to M.I.

Reprints and permission information is available at http://www.nature.com/reprints

Publisher's note Springer Nature remains neutral with regard to jurisdictional claims in published maps and institutional affiliations.